

## Electrodeposited epitaxial Fe<sub>100-x</sub>Co<sub>x</sub> films on *n*-GaAs (100)

J. J. Mallett, E. B. Svedberg, M. D. Vaudin, L. A. Bendersky, A. J. Shapiro, W. F. Egelhoff, Jr., and T. P. Moffat  
*Materials Science and Engineering Laboratory, National Institute of Standards and Technology, Gaithersburg, Maryland 20899, USA*  
 (Received 19 September 2006; revised manuscript received 6 December 2006; published 6 February 2007)

The electrodeposition of epitaxial cube-on-cube Fe<sub>100-x</sub>Co<sub>x</sub> films onto (100)-oriented *n*-GaAs from ferrous ammonium sulfate solutions containing various concentrations of cobalt sulfate is described. The cobalt composition in a series of 400-nm-thick films was found to vary in proportion to the concentration of cobalt sulfate in the electrolyte and six compositions in the range from 0 to 74% were deposited. Epitaxial (100)-oriented bcc films were produced throughout this range, as suggested by symmetrical x-ray diffraction and confirmed by x-ray pole figure measurements. Rocking curve measurements yielded data that could be fitted to the sum of a Lorentzian and a Gaussian, corresponding to the (200) Fe<sub>100-x</sub>Co<sub>x</sub> planes and to a residual contribution from GaAs (400), respectively. The full width at half maximum obtained for the film Lorentzians varied from 0.44° to 0.90° and was apparently uncorrelated with composition. X-ray (211) pole figure measurements revealed a high degree of twinning of the (100) bcc Fe<sub>100-x</sub>Co<sub>x</sub> consistent with a recent study of Fe films electrodeposited on *n*-GaAs.

DOI: 10.1103/PhysRevB.75.085304

PACS number(s): 81.15.Pq, 61.10.Nz, 68.55.Jk

### I. INTRODUCTION

Spin-electronics offers the promise of combining the non-volatility of magnetic data storage and/or the sensor capabilities of giant magnetoresistance and magnetic tunnel junctions with established electronic device structures.<sup>1-4</sup> The injection of spin from the ferromagnetic material to the semiconductor (whether it be directly or through a tunnel barrier) is enhanced by an epitaxial layer of ferromagnetic material within the spin coherence length of the interface between them. Fe has a body-centered-cubic (bcc) crystal structure with a lattice parameter of 0.2866 nm and GaAs has a face-centered-cubic (fcc) crystal structure with a lattice parameter of 0.5654 nm; thus the two crystal lattices match well in a cube-on-cube orientation, with a mismatch of 1.4%. It has been recently demonstrated that iron can be electrodeposited epitaxially cube-on-cube onto GaAs in the presence of ammonium sulfate.<sup>5-7</sup> Other groups have reported varying degrees of (100) texture depending on anion type and plating conditions.<sup>8</sup> The quality of these films, as characterized by rocking curve measurements, equals that of vacuum deposited films. On the other hand, Co electrodeposited onto GaAs has been found to produce mainly hcp films with two competing crystallographic orientations.<sup>9</sup> The phase diagram for Fe<sub>100-x</sub>Co<sub>x</sub> indicates a stable single-phase bcc region from 0-at. % Co to close to 80%. Furthermore, the lattice mismatch of Fe<sub>100-x</sub>Co<sub>x</sub> with GaAs improves from 1.4% to 0.5% over this range of composition. The possibility of improved cube-on-cube epitaxy with increasing Co content (up to 80%) was therefore anticipated. There are also significant advantages of alloying Co with Fe in terms of magnetic properties. The Fe<sub>67</sub>Co<sub>33</sub> alloy corresponds to the highest known intrinsic induction of any material (2.4 T).<sup>10</sup> Perhaps more importantly for spintronic applications, the spin polarization at the Fermi level determined from band-structure calculations increases significantly with cobalt fraction.<sup>11</sup>

### II. EXPERIMENT

Suitable substrates for electrodeposition were prepared by diffusing GaIn eutectic through the back surface of (100)

*n*-GaAs wafer fragments to form Ohmic contacts. Substrates were masked using electroplating tape leaving a 5-mm-diameter area of the front surface of the GaAs exposed. This was etched in 7.2 mol/L ammonium hydroxide for 30 s and rinsed in deionized water for 60 s immediately prior to deposition. A series of six 400-nm Fe<sub>100-x</sub>Co<sub>x</sub> films was electrodeposited at a constant current density of 10 mA/cm<sup>2</sup> from aqueous solutions containing 100-mmol/L FeSO<sub>4</sub> and 30-mmol/L NH<sub>4</sub>SO<sub>4</sub>. The thickness of the films was confirmed to within 5% by measuring the difference in mass of the sample before and after deposition. The concentration of CoSO<sub>4</sub> was increased from 0 mol/L to 400 mmol/L in five steps, to produce a proportionally increasing series of Co atomic fractions of 0, 0.16, 0.36, 0.53, 0.64, 0.74, as determined by energy dispersive x-ray spectroscopy. This is in agreement with previous reports of Fe<sub>100-x</sub>Co<sub>x</sub> electrodeposition from ammonium sulfate solutions.<sup>12-14</sup> X-ray-diffraction measurements were carried out with two diffractometers, one a powder diffractometer with a germanium monochromator tuned to only pass through the CuKα<sub>1</sub> wavelength, and the other a four-circle diffractometer equipped with a point detector and an area detector. The latter is configured horizontally with the ω and 2θ axis vertical. The sample stage rotates about these axes and is equipped with χ and φ rotation capabilities. The collimated incident x-ray beam used for the area detector measurements had a 0.5 mm diameter. The shape and size of the x-ray spot generated by this beam on the sample depended upon the angle of incidence, but was generally oval with major and minor axes between 0.5 and 1 mm. The impinging x-ray beam used for the other measurements was significantly broader, covering the whole sample area.

### III. RESULTS AND DISCUSSION

The symmetrical (θ-2θ) x-ray diffraction data shown in Fig. 1 reveal large (~2000 counts/s) Fe<sub>100-x</sub>Co<sub>x</sub> (200) peaks overlapping with GaAs (400) for all films in the series except the Fe<sub>26</sub>Co<sub>74</sub> sample [Fig. 1(f)]. For this sample, a (110)

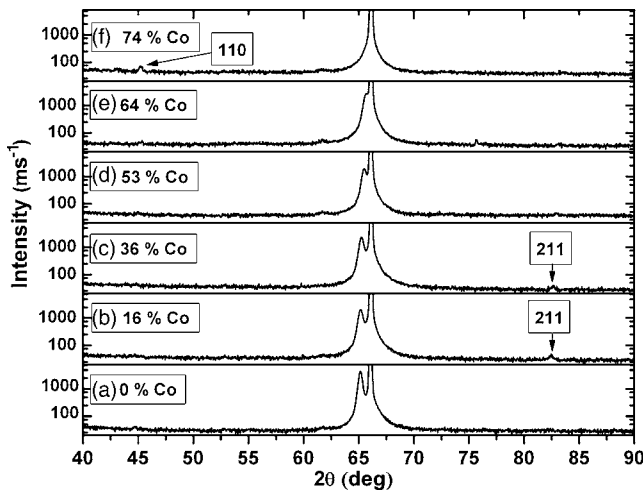


FIG. 1. A series of  $(\theta-2\theta)$  plots taken using monochromatic x rays in the Bragg-Brentano symmetrical geometry. The film (200) peaks close to  $65.2^\circ$  overlap with the GaAs substrate (400) peaks increasingly with Co fraction. Minor additional film peaks are marked where present. (Note the logarithmic vertical scale.)

peak is clearly evident at 15 counts/s above the noise level, but was absent from the diffraction data obtained for the other samples. The  $\text{Fe}_{84}\text{Co}_{16}$  and  $\text{Fe}_{64}\text{Co}_{36}$  films produced small (45 counts/s) (211) peaks as marked in Figs. 1(b) and 1(c), in addition to much larger (1800 counts/s) (200) peaks. In order to most clearly resolve the  $\text{Fe}_{100-x}\text{Co}_x$  (200) from the GaAs (400), reciprocal space maps were generated using the four-circle diffractometer using the point detector. A small region of reciprocal space around the GaAs 400 pole (and the film 200 pole) was sampled by systematically rotating the detector while rotating the specimen in  $\chi$  and  $\omega$ . The reciprocal space maps recorded x-ray intensity as a function of reciprocal lattice position in two dimensions ( $h$  and  $l$ ), but the small-angle approximation allowed them to be interpreted as a series of  $\theta-2\theta$  plots taken at different sample tilts, from which it was possible to choose a tilt that significantly attenuated the GaAs (400) peak, while maintaining a reasonable intensity of the  $\text{Fe}_{100-x}\text{Co}_x$  bcc (200) peak. [This was effective because of the better alignment of (100) planes in the GaAs substrate than the film.] Examples for the six films measured are shown in Fig. 2, where the  $\theta-2\theta$  plots were extracted from reciprocal-space-map data corresponding to a sample tilt  $\omega$  of approximately  $0.16^\circ$  about the axis orthogonal to the diffraction plane. (Single columns of data from the reciprocal space maps were actually used, corresponding to a constant reciprocal space parameter  $l$ , but this corresponds closely to a constant  $\omega$  to within 0.03%.) The GaAs (400) peaks in Fig. 2 at  $66.1^\circ$  have been attenuated from over 100 000 counts/s in the symmetrical diffraction condition to approximately 2000 counts/s by the  $0.16^\circ$  sample tilt. A series of  $\text{Fe}_{100-x}\text{Co}_x$  (200) peaks is resolved at lower angles, shifting progressively towards the GaAs (400) peak with increasing Co fraction. The curves shown in Fig. 2 are in each case the sum of two Lorentzians centered at two different angles and with two different widths, corresponding to diffraction from the film and substrate, respectively. This allowed diffraction from the film to be clearly separated from

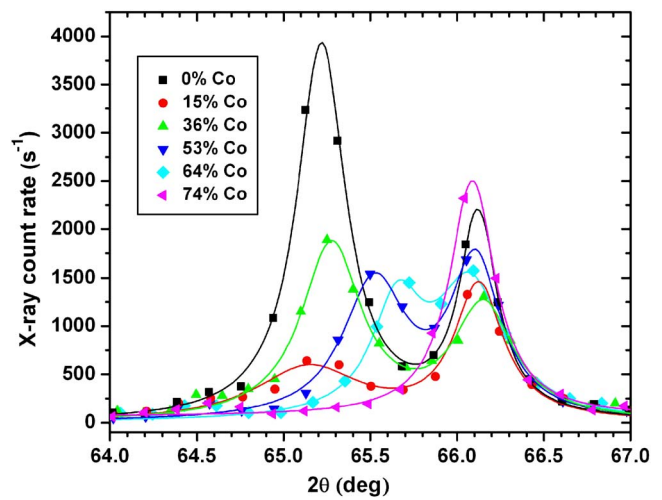


FIG. 2. (Color online) A series of  $(\theta-2\theta)$  plots extracted from reciprocal space maps, showing the shift in the film (200) peaks towards the GaAs (400) with increasing Co fraction. The GaAs substrate (400) peak has been intentionally attenuated considerably more than that of the film due to the sample tilt.

that of the substrate in all cases except for the  $\text{Fe}_{26}\text{Co}_{74}$  sample. In that case the optimum fit was achieved with a single Lorentzian. This failure to resolve the  $\text{Fe}_{26}\text{Co}_{74}$  sample peak may be due to the small (0.5%) lattice mismatch at this composition, or may be indicative of an absence of cube-on-cube epitaxy at this composition. Notwithstanding the ambiguity of the  $\text{Fe}_{26}\text{Co}_{74}$  sample, the resolved  $\text{Fe}_{100-x}\text{Co}_x$  (200) peaks shown in Fig. 2 indicate at the very least a strong (100) texture for the remaining films and suggest cube-on-cube epitaxy.

In addition to the information shown in Fig. 2, the reciprocal space maps also provided data analogous to a series of rocking curves, as shown in Fig. 3. Rows of x-ray intensity data corresponding to constant reciprocal space parameter  $h$  were taken from the reciprocal space maps, closely approximating (to within 0.03%) constant  $2\theta$  values near to the diffraction maxima shown in Fig. 2. In all cases the rocking curves were fitted to the sum of a narrow Gaussian and a broad Lorentzian, corresponding to the GaAs substrate and film, respectively. The full width at half maximum (FWHM) of the Gaussian component was close to  $0.036^\circ$  in all cases. This was consistent with the width of rocking curves obtained for the substrate alone. It is also close to the  $0.03^\circ$  angular resolution limit of the diffractometer configuration. The Gaussian profile is also consistent with exclusively instrumental broadening. The magnitude of the Gaussian contribution from the GaAs (400) increases with Co content due to the increasing proximity of the GaAs (400) spike to the film (200) peak in reciprocal space. The somewhat broader Lorentzian component is present in all cases and is attributed to the films. The FWHM of the Lorentzians is marked next to the curves in Fig. 3. The average value of  $0.65^\circ$  is typical of Fe films deposited onto GaAs by various methods. There does not appear to be a systematic trend in the FWHM values with composition. The apparently random variation in FWHM between films is much larger than the statistical error of approximately 1% suggested by the fitting process. It may

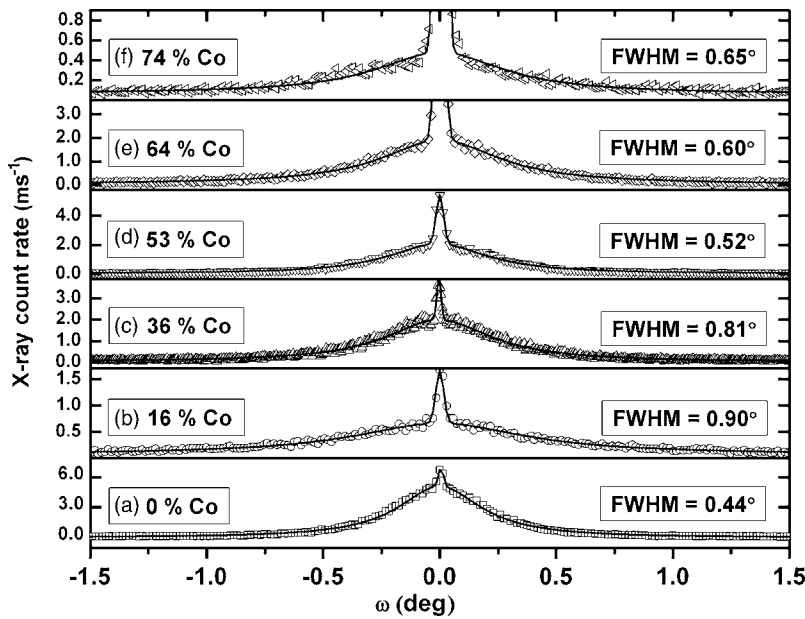


FIG. 3. Rocking curves extracted from reciprocal space maps of the  $\text{Fe}_{100-x}\text{Co}_x$  films. The fits are the sum of a Gaussian (GaAs substrate) and Lorentzian (film) and the quoted full width half maxima correspond to the film.

indicate a degree of dispersion in the initial surface states of the GaAs substrates. It may be significant that the films with the widest rocking curves are the  $\text{Fe}_{26}\text{Co}_{74}$  and the  $\text{Fe}_{84}\text{Co}_{16}$ , which also exhibited the low intensity (110) and (211) peaks, respectively, as noted above. The integrated areas of the Lorentzian component of the rocking curves for those two films are also less than a half of the average, suggesting significantly less epitaxial material in these cases. The presence of the Lorentzian characteristic of (100) film texture is especially noteworthy in the case of the  $\text{Fe}_{26}\text{Co}_{74}$ , for which a (200) peak could not be resolved in Fig. 2.

The measurements discussed thus far are a strong indication of an almost exclusive (100) orientation of the films parallel to the plane of the substrate. This is consistent with the anticipated cube-on-cube texture, but does not prove it (fiber texture remains a possibility). In order to investigate further the in-plane texture of the films, an area detector was used with the four-circle diffractometer to collect nonsymmetric x-ray data. The sample was rotated  $26^\circ$  away from vertical about the (horizontal)  $\chi$  axis and data were collected while the sample was rotated about the  $\phi$  axis normal to the sample surface. The initial ( $\phi=0$ ) setting of the sample was with one of the cleaved  $\langle 110 \rangle$  edges horizontal. The  $\omega$  setting was equal to the Bragg angle for Fe (211), and  $2\theta$  was set to twice that.

Seventy-two successive area detector frames were measured in this configuration while rotating the sample azimuthally through  $360^\circ$  about the  $\phi$  axis. As expected, four  $\{422\}$  GaAs planes were successively brought into the Bragg condition, one every  $90^\circ$  of azimuthal sample rotation. Fainter  $\text{Fe}_{100-x}\text{Co}_x$  (211) reflections were also detected in the same frames as the GaAs (422) reflections, for all but the most Co rich film, showing cube-on-cube epitaxy between the Fe and GaAs. The diffractometer software gives  $2\theta$  and  $\chi$  values for any position on the area detector and it was found that the film and GaAs spots corresponded to slightly different  $d$  spacings. This is illustrated in Fig. 4(a), which shows one such area detector frame taken from the  $\text{Fe}_{64}\text{Co}_{36}$  film, in

which the axis of separation of the Fe and GaAs is marked  $2\theta$ . Note that there is no separation of the spots along the orthogonal axis on the area detector (marked  $\chi$ ), which suggests zero average tilt of this component of the film with respect to the substrate. This is consistent with Figs. 2 and 3, demonstrating out-of-plane (100) orientation. (It is not strictly correct to show orthogonal Cartesian  $2\theta$  and  $\chi$  axes, since lines of constant  $2\theta$  and  $\chi$  on the detector are conic sections rather than Cartesian in nature. For the geometry chosen, however, the axes marked in Fig. 4 are a reasonable approximation for illustrative purposes.) The measurements described below were obtained from proprietary software, provided by the manufacturer of the diffractometer, and took full account of the more complex geometry.) The fact that the  $\text{Fe}_{100-x}\text{Co}_x$  (211) spots appear in the same frame (i.e., the same  $\phi$ ) as the GaAs (422), proves the anticipated *in-plane* (azimuthal) orientation and the cube-on-cube epitaxy. During the measurements of all samples except the most Co rich, a second series of eight spots appeared in different frames to the GaAs (422). One of those eight frames is shown in Fig. 4(b), once again for the  $\text{Fe}_{64}\text{Co}_{36}$  film. The position of the spot in Fig. 4(b) is at an identical  $2\theta$  value to that of the cube-on-cube  $\text{Fe}_{100-x}\text{Co}_x$ , proving it to be from material of the same lattice spacing, but differing in  $\chi$  by  $18^\circ$ . The information from the area detector concerning the diffraction from the (221) planes of  $\text{Fe}_{100-x}\text{Co}_x$  is best presented as partial (221) pole figures, as shown in Fig. 4. These figures were generated by integrating across the narrow regions of the area detector corresponding to  $\text{Fe}_{100-x}\text{Co}_x$  (211) diffraction (the center boxes in Fig. 4) and plotting the values as a function of  $\chi$ ; note that the outer boxes are for background subtraction. The integration allowed most of the intensity of the  $\text{Fe}_{100-x}\text{Co}_x$  (211) diffraction to be captured, but was confined to a sufficiently narrow region to prevent the inclusion of diffraction from the GaAs (422) planes, as shown by the position of the center box in Fig. 4. The integration of the 72 frames captured for each sample provided 72 radial segments for the corresponding pole figure, the position of each seg-

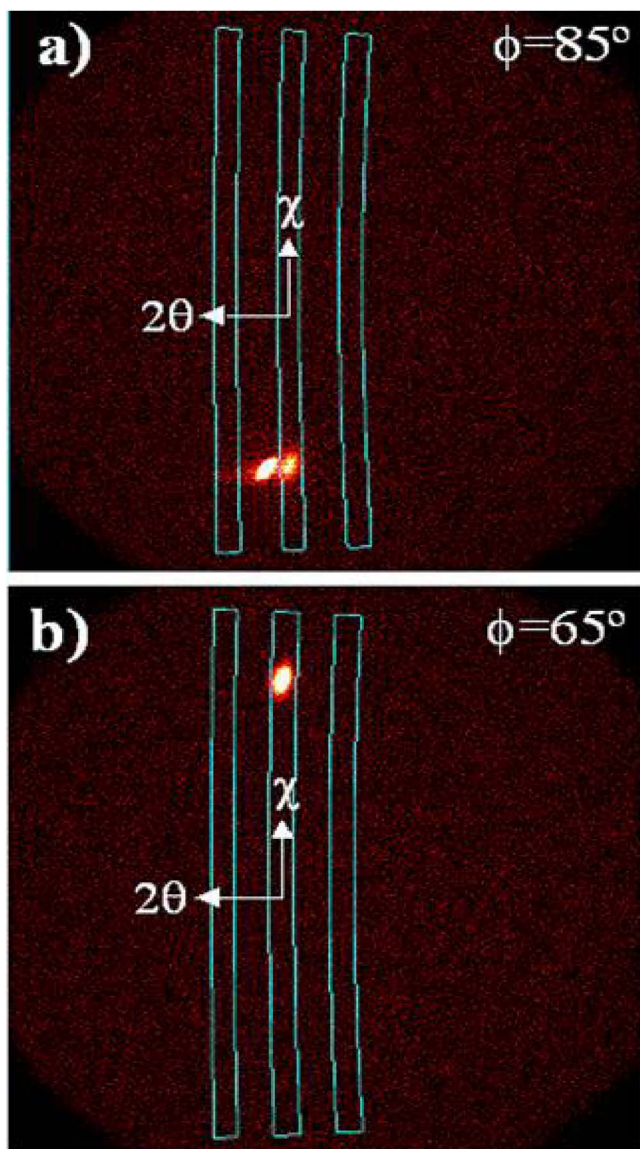


FIG. 4. (Color online) The area detector frames taken with the sample azimuthally rotated to (a)  $\phi=85^\circ$  and (b)  $\phi=65^\circ$ . The position of features along the horizontal axis marked  $2\theta$  is a measure of the spacing of the diffracting planes. The position of a feature on the vertical axis marked  $\chi$  is an indication of the tilt of the diffracting planes. The intense and less intense features in (a) correspond to diffraction from (422) planes in the GaAs substrate and (211) planes in the  $\text{Fe}_{64}\text{Co}_{36}$  film, respectively. The film spot contains contributions from (211) (twin) planes of both the cube-on-cube and twin grains. The feature in (b) corresponds to diffraction from (211) planes in the twin grains only.

ment in the pole figure corresponding to the azimuthal rotation of the sample when the frame was captured. The intensity at each point along a segment is displayed as a gray scale in the pole figures shown in Fig. 5. These figures provide a useful summary of diffraction from  $\text{Fe}_{100-x}\text{Co}_x$  (211) planes over a wide range of orientations in the sample. The radial distance from the center of the pole figure corresponds to the tilt of the measured (221) planes from the sample plane. The width of the annulus shown in the pole figure is determined

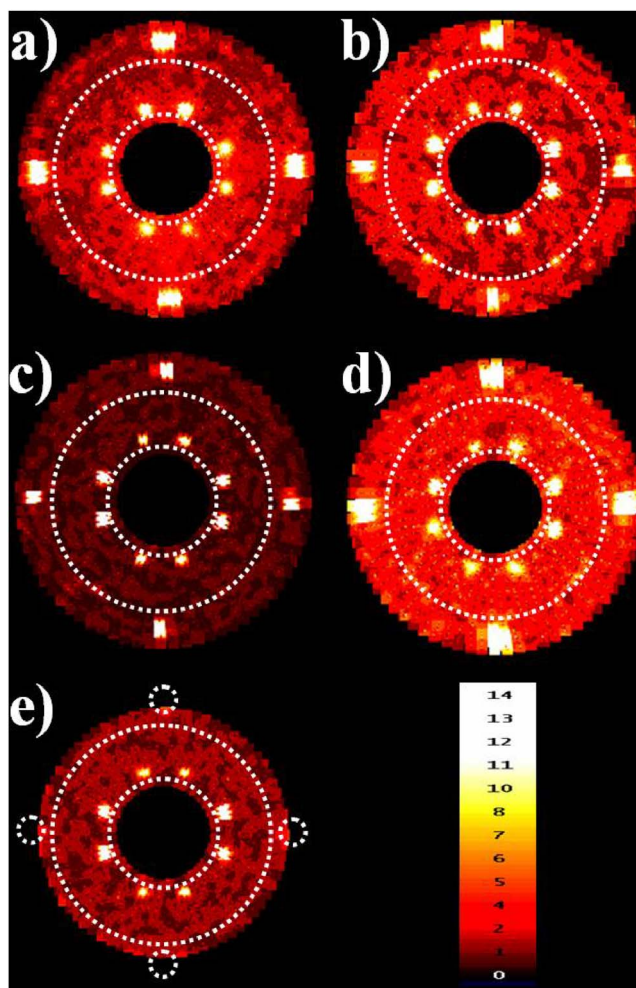


FIG. 5. (Color online) 211 pole figures taken for films containing (a) 0%, (b) 16%, (c) 36%, (d) 53%, and (e) 64% Co. The concentric dotted white circles represent tilts of the 211 planes of  $15^\circ$  and  $30^\circ$ , respectively. The color (grey) scale is in units of counts. The small circles in (e) represent the position of the additional film spots, which could not be deconvolved from the GaAs (400) and were therefore not shown. The pole figure from the 74% Co film is not shown as it showed no features that could be deconvolved from those of GaAs.

by the diameter of the area detector and its separation from the sample. This annulus covers all (211) planes tilted between  $13^\circ$  and  $35^\circ$  from the sample plane. The azimuthal angle between features on the pole figures corresponds to their in-plane rotation with respect to each other. The spots near the outer edge of the pole figures shown in Figs. 5(a)–5(d) are from  $\text{Fe}_{100-x}\text{Co}_x$  (211) planes tilted  $35.3^\circ$  from the sample plane. This tilt and their azimuthal separation of  $90^\circ$  are consistent with cube-on-cube  $\text{Fe}_{100-x}\text{Co}_x$ . The corresponding spots in Fig. 5(e) are depicted as dotted circles, because it was not possible to clearly separate the  $\text{Fe}_{36}\text{Co}_{64}$  cube-on-cube (211) film reflections from the GaAs (422) in this case. (An asymmetry in the shape of the combined  $\text{Fe}_{36}\text{Co}_{64}$  and GaAs spot in the appropriate area detector frames was, however, seen, indicating the presence of cube-on-cube  $\text{Fe}_{36}\text{Co}_{64}$ .) Evidence of cube-on-cube epitaxy could not be found for the  $\text{Fe}_{26}\text{Co}_{74}$  films. The pole figure corre-

sponding to this film was featureless and so is not presented in Fig. 5.

In each of the pole figures (except the featureless one taken for  $\text{Fe}_{26}\text{Co}_{74}$ ) there is a second set of eight spots at a radius corresponding to a tilt of  $17.7^\circ$ . These correspond to  $\text{Fe}_{100-x}\text{Co}_x$  oriented with the  $[221]$  direction parallel to the surface normal. This is most readily explained as twinning of the cube-on-cube material and has been noted elsewhere for electrodeposited Fe-GaAs.<sup>7</sup> The very specific orientation of the (211) planes in the twinned material demonstrated in the pole figures by the sharpness of the inner (211) spots is a further indication of the quality of the epitaxy of the cube-on-cube material from which it was derived. The absence of the twin spots in the pole figure taken from the  $\text{Fe}_{26}\text{Co}_{74}$  film (not shown) throws further doubt on the existence of cube-on-cube material for this film. It remains possible, however, that the excellent lattice match of a film of this composition with GaAs prevents resolution of the cube-on-cube diffraction from the substrate and that the reduced strain reduces or eliminates twinning. It should be noted that minor streaking appeared in the area detector frames taken for the  $\text{Fe}_{26}\text{Co}_{74}$  film along the region of the frame corresponding to (211) diffraction. Its presence suggests a degree of randomly oriented material consistent with the presence of the (110) peak noted above from symmetrical diffraction. No evidence of random orientations was found for any of the other films. Additional faint spots are, however, evident in the case of the  $\text{Fe}_{84}\text{Co}_{16}$  film [Fig. 5(b)], which are in the appropriate position for (211) oriented grains, consistent with the small (211) peak reported above from the symmetrical  $\theta$ - $2\theta$  diffraction.

It is important to note that the (221) (twinned) material also produces spots on the pole figure that exactly coincide with the cube-on-cube spots. This is obviously a complication in determining the volume ratios of twinned to epitaxial  $\text{Fe}_{100-x}\text{Co}_x$ . It does not invalidate our conclusions thus far concerning the existence of cube-on-cube material, however, since Fig. 2 proves the existence of  $\text{Fe}_{100-x}\text{Co}_x$  oriented with the (001) planes parallel to the surface, and the existence of the outer spots rather than rings at this radius precludes the possibility of (001) fiber texture. Separation of the contributions to the outer spots from the two orientations is possible by careful consideration of the azimuthal symmetry of the *magnitudes* of the features in the pole figure.

This was performed in two stages. The first step of selecting two annuli from each pole figure and integrating over their  $5^\circ$  width was used to generate  $\phi$  scan graphs of the type shown in Fig. 6. Figure 6 corresponds to the  $\text{Fe}_{64}\text{Co}_{36}$  film and is typical of all the films studied. The dashed curve taken from the inner spots of the pole figure corresponds exclusively to twinned grains with a (221) out-of-plane orientation. The fourfold symmetry in the *positions* of the peaks and their relative angular offsets provide useful confirmation of the assignment of this orientation. The reduced uniaxial symmetry in the *magnitudes* of the peaks in this curve indicates different volume fractions of orthogonal twin variants. This suggests that the twinning occurs more readily along one crystallographic direction on the GaAs than in the orthogonal direction. This may be correlated with the miscut of the GaAs leading to a preferred step edge direction, or may be related to the surface termination of the GaAs, which has

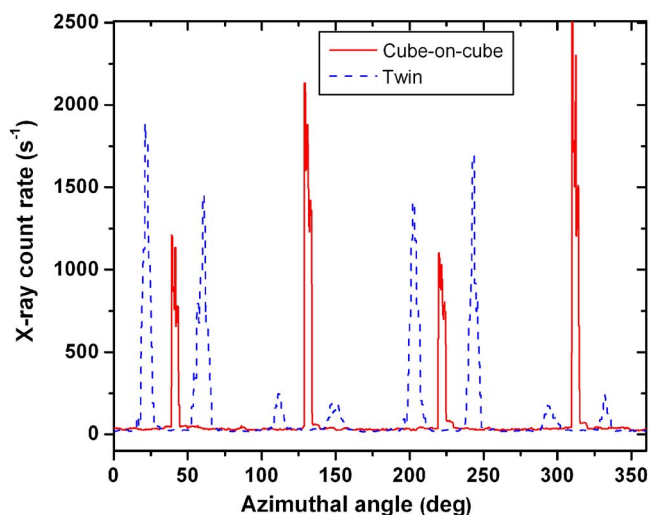


FIG. 6. (Color online) The total intensities averaged over the widths of two annuli placed on Fig. 5(c) to cover the inner and outer spots, respectively. The blue (dotted) line corresponding to the inner spots is labeled twin only and shows the high degree of asymmetry in the number of orthogonal twin variants. The red (solid) line corresponds to the outer spots and contains a contribution from twinned and cube-on-cube material.

been reported to induce a uniaxial strain during the early stages of film growth.<sup>15,16</sup> The ratio of the volume fractions of one twin variant to the orthogonal was found to be 5:1 by comparing the peak areas. The second (solid) curve in Fig. 6 is taken from the outer spots of the pole figure and corresponds to equally weighted contributions from cube-on-cube and twin grains. The cube-on-cube grains, like the underlying GaAs substrate necessarily produce spots on the pole figure with fourfold symmetry in both *magnitude* and *position*. [This was confirmed for the GaAs substrate by comparing four (400) spots from a GaAs (422) pole figure, all of which contained the same number of counts to within 2%, showing that any lack of fourfold symmetry in the pole figure is due to differing twin variant volumes, rather than sensitivity or alignment variations in the diffractometer. Many  $\phi$  scans performed with point detectors do indeed show variations in symmetrically equivalent features that are simply due to imperfect alignment of the axes of rotation. Measurements derived from an area detector, however, are less prone to this problem, as minor misalignments simply cause offsets in the positions of the features on the area detector.] The asymmetry in the *magnitudes* of the peaks in the curve taken from the outer spots is therefore entirely due to the contribution from the twin material and not related to instrumental issues. The ratio of the contributions from the orthogonal twin variants to the outer spots was assumed to be the same as that of the inner spots (5:1). This knowledge combined with the actual areas of the outer peaks enabled the contributions from the cube-on-cube and twin to be separated using simultaneous equations. A value of 4905 counts was obtained for the cube-on-cube material, while 4854 and 916 were obtained for the two twin variants. These values are directly comparable, since they correspond to x-ray measurements of (211) planes oriented in exactly the same way in

TABLE I. The ratios of the volumes of orthogonal twin variants obtained from integrated pole figure x-ray intensities and the cube-on-cube to twin volume ratio determined as described in the text.

Atomic fraction Co (%)	Ratio of orthogonal twin variant volumes	Average ratio of cube-on-cube to twin volumes
0±0	2.5±0.5	0.67±0.20
16±2	2.6±0.6	0.48±0.21
36±2	5.3±0.3	0.84±0.15
54±2	1.5±0.1	1.10±0.4
64±2	2.5±0.5	

both variants. [The coincidence of the twin and cube-on-cube spots at 35.5° occurs because the (211) planes that produce those spots are twin planes in the Fe<sub>100-x</sub>Co<sub>x</sub>.] The usual corrections for differences in x-ray absorption (due to path length), or for structure factor, are not needed when comparing the above numbers with each other and between samples of the same thickness measured using the same setup. Table I gives the values of the ratios of volume fractions of the orthogonal twin variants measured directly by integrating the inner spots of the pole figures shown in Fig. 5. It also gives the ratios of the cube-on-cube to twin volume fractions derived in the way described above for the Fe<sub>64</sub>Co<sub>36</sub> film. The ratio of the twin variants varies substantially from sample to sample, but the ratio of twinned to cube-on-cube volume fraction remains constant within error. This suggests that the degree of twinning remains invariant with film composition. (The errors were obtained from differences in the areas of peaks corresponding to the same twin variant, which are attributed to noise. The error in the determination of the cube-on-cube to twin ratio for the Fe<sub>46</sub>Co<sub>54</sub> film was especially high, due to the smaller ratio between the variants. This made the percentage difference between the outer spot intensities relatively small for this sample, amplifying the statistical error in separating the contributions to the outer spots from the cube-on-cube material.) It should be noted that x-ray pole figure measurements (not used here) of 400-nm Fe films deposited onto different GaAs wafers showed substantial variations in the ratio of cube-on-cube to twin volume (between 0.5 and 3). The small variation in the values shown in the final column of Table I may be due to the fact that all samples were deposited onto the same wafer.

The lattice spacings for the Fe<sub>100-x</sub>Co<sub>x</sub> films extracted from various x-ray measurements (solid symbols) are compared with bulk values<sup>17</sup> (open symbols) in Fig. 7. Values corresponding to out-of-plane spacing were extracted from the diffraction data shown in Figs. 1 and 2. In addition measurements were taken from diffraction spots in the area detector frames used to generate the pole figures. In every case, the nearest GaAs peak was used as an internal calibration. The lattice parameters obtained for the films using different x-ray measurements agree to better than 0.15%. Values taken from twin grains using the area detector are indistinguishable from those of cube-on-cube material from symmetrical measurements. The lattice parameters follow the same trend with composition as those of bulk films taken from the literature,

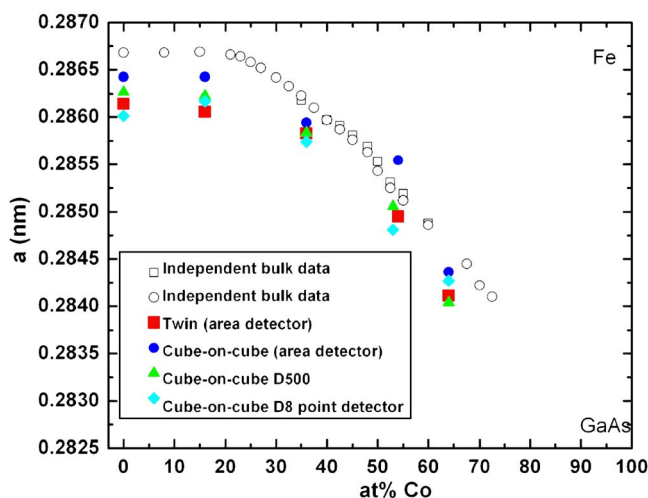


FIG. 7. (Color online) The lattice spacings obtained from measurements of thin Fe<sub>100-x</sub>Co<sub>x</sub> films (solid symbols) compared with bulk values.

decreasing with increasing cobalt fraction. The small offset between the lattice spacings of bulk Fe<sub>100-x</sub>Co<sub>x</sub> and of the electrodeposited films is larger than the statistical error and is unlikely to be due to systematic error common to three different diffraction geometries and two different diffractometers, especially considering the internal calibration obtained from the GaAs substrate. The lattice misfit between the cube-on-cube films and the GaAs substrate would be expected to produce a compressive strain in the former. This would then be expected to result in an expansion of the out-of-plane lattice spacing, rather than the observed compression. The same phenomenon has been observed by Bao *et al.*<sup>5,6</sup> for FeNi films electrodeposited onto GaAs. In both cases it may be due to incorporation of impurities into the electrodeposited films.

Cross-sectional TEM images were obtained from a 200-nm-thick Fe film deposited under the same conditions as described above for the samples used for the x-ray studies.

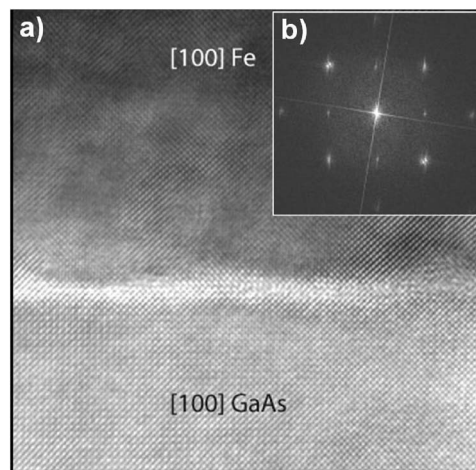


FIG. 8. A cross sectional TEM image (a) of an Fe film on GaAs showing cube-on-cube epitaxy. The Fourier transform of the image is shown in (b).

Figure 8(a) shows such an image, taken to include the interface of the film and substrate. The Fourier transform displayed in Fig. 8(b) shows almost coincident Fe and GaAs lattices. Careful examination of the bright spots at the top left and bottom right reveals that they are comprised of two spots each, closely spaced. The spacing is due to the 1.4% mismatch between the film and substrate.

#### IV. CONCLUSIONS

$\text{Fe}_{100-x}\text{Co}_x$  films were electrodeposited onto *n*-GaAs from ferrous ammonium sulfate solutions containing different concentrations of cobalt sulfate. The film composition was found to vary in proportion with the cobalt content of the plating solution in agreement with previous studies<sup>12-14</sup>. Symmetrical x-ray-diffraction measurements resolved substantial  $\text{Fe}_{100-x}\text{Co}_x$  (200) peaks from the GaAs substrate (400) peaks for films with Co fractions of up to 0.64, constituting strong evidence of (100) texture over this range of compositions. The failure to resolve a (200) peak in the case of the 74% Co film may have been due its proximity to the substrate peak. Rocking curve measurements around the  $\text{Fe}_{100-x}\text{Co}_x$  (200) peaks produced FWHM of between  $0.44^\circ$  and  $0.9^\circ$ , indicat-

ing a narrow distribution of out-of-plane orientations around (200). X-ray 211 pole figures contained the anticipated four-fold symmetrical features consistent with cube-on-cube epitaxy, but also revealed evidence of (221) oriented material most readily attributable to first-order twinning of the epitaxial cube-on-cube component. This was deduced from the position and rotational symmetry of features appearing on the pole figure at a radius corresponding to  $17.5^\circ$  tilt of the (211) planes. The uniaxial symmetry of the magnitudes of these features indicated a disparity in the quantity of the two orthogonal twin variants. The corresponding asymmetry in features common to both twin and cube-on-cube material was used to estimate the volume fractions of both phases.

The evidence presented above suggests that high quality cube-on-cube epitaxy of  $\text{Fe}_{100-x}\text{Co}_x$  on GaAs may be possible over a wide range of Co fractions. The existence of twinning in these thick films may not necessarily be detrimental to spintronic applications, for which the quality of the epitaxy within the spin coherence length of the GaAs-film interface is pertinent. Further work addressing the distribution of the twin volume is underway. The ability to deposit high quality epitaxial bcc films with high cobalt content is anticipated to facilitate spin injection.

<sup>1</sup>M. Johnson, *J. Phys. Chem. B* **109**, 14278 (2005).

<sup>2</sup>S. van Dijken, X. Jiang, and S. S. P. Parkin, *Phys. Rev. Lett.* **90**, 197203 (2003).

<sup>3</sup>S. van Dijken, X. Jiang, and S. S. P. Parkin, *Phys. Rev. B* **66**, 094417 (2002).

<sup>4</sup>G. Wastlbauer and J. A. C. Bland, *Adv. Phys.* **54**, 137 (2005).

<sup>5</sup>Z. L. Bao and K. L. Kavanagh, *J. Appl. Phys.* **98**, 066103 (2005).

<sup>6</sup>Z. L. Bao, Ph.D. thesis, Simon Fraser University, Vancouver, 2006.

<sup>7</sup>E. B. Svedberg, J. J. Mallett, L. A. Bendersky, A. G. Roy, W. F. Egelhoff, Jr., and T. P. Moffat, *J. Electrochem. Soc.* **153**, 807 (2006).

<sup>8</sup>Y.-K. Liu, C. Scheck, R. Schad, and G. Zangari, *Electrochem. Solid-State Lett.* **7**, D11 (2004).

<sup>9</sup>A. Ford, J. E. Bonevich, R. D. McMichael, M. D. Vaudin, and T. P. Moffat, *J. Electrochem. Soc.* **150**, C735 (2003).

<sup>10</sup>I. Shao, L. Romankiw, E. I. Cooper, and C. Bonhote, *Proc.-Electrochem. Soc.* **PV 2004-17**, 420 (2004).

<sup>11</sup>K. Schwarz, P. Mohn, P. Blaha, and J. Kubler, *J. Phys. F: Met. Phys.* **14**, 2659 (1984).

<sup>12</sup>E. M. Kakuno, D. H. Mosca, I. Mazzaro, N. Mattoso, W. H. Schreiner, and M. A. B. Gomes, *J. Electrochem. Soc.* **144**, 3222 (1997).

<sup>13</sup>M. Mattoso, V. Fernandes, M. Abbate, W. H. Schreiner, and D. H. Mosca, *Electrochem. Solid-State Lett.* **4**, C20 (2001).

<sup>14</sup>I. Shao, P. M. Vereecken, C. L. Chien, R. C. Cammarata, and P. C. Searson, *J. Electrochem. Soc.* **150**, C184 (2003).

<sup>15</sup>M. Brockmann, M. Zöfl, S. Miethaner, and G. Bayreuther, *J. Magn. Magn. Mater.* **198-199**, 384 (1999).

<sup>16</sup>O. Thomas, Q. Shen, P. Schieffer, N. Tournerie, and B. Lepine, *Phys. Rev. Lett.* **90**, 017205 (2003).

<sup>17</sup>J. G. Parr, *J. Iron Steel Inst., London* **205**, 426 (1967).